Understanding the gap in polyoxovanadate molecule-based magnets

A. Barbour,[1] R. D. Luttrell,[1] J. Choi,[1] J. L. Musfeldt,[1] D. Zipse,[2] N. S. Dalal,[2] D. W. Boukhvalov,[3] V. V. Dobrovitski,[7] M. I. Katsnelson,[5] A. I. Lichtenstein,[6] B. N. Harmon,[7] and P. Kögerler[7]

[1]*Department of Chemistry, University of Tennessee, Knoxville, Tennessee 37996, USA*

[2]*Department of Chemistry and Biochemistry, National High Magnetic Field Laboratory, and Center for Materials Research and Technology, Florida State University, Tallahassee, Florida 32306, USA*

[3]*Institute of Metal Physics, Russian Academy of Sciences Ural Division, Ekaterinburg 620041, GSP-170, Russia*

[4]*Ames Laboratory, Iowa State University, Ames, Iowa 50011, USA*

[5]*Institute for Molecules and Materials, Radboud University Nijmegen, Toernooiveld 1, 6525 ED Nijmegen, The Netherlands*

[6]*Institut für Theoretische Physik, Universität Hamburg, 20355 Hamburg, Germany*

[7]*Ames Laboratory, Iowa State University, Ames, Iowa 50011, USA*

(Received 18 January 2006; revised manuscript received 25 April 2006; published 12 July 2006)

We report a joint experimental and theoretical investigation of the transport gap, optical properties, and electronic structure of two chemically similar, inhomogeneously mixed-valent polyoxovanadate molecule-based magnets. We attribute the substantial gap in $[NHEt_3]_4[V_8^{IV}V_4^{V}As_8O_{40}(H_2O)]\cdot H_2O$ to weak *p-d* hybridization and a large on-site Coulomb repulsion ($U=6$ eV). The reduced gap in $[NHEt_3]_3[V_6^{IV}V_6^{V}As_8O_{40}(HCO_2)]\cdot 2H_2O$ is associated with a smaller value of U (4 eV), at least from a molecular point of view, although the transport properties also reflect subtle organization of the molecular structure and differences between direct and indirect intermolecular charge transfer. A detailed analysis of the vibrational response supports the important role of local molecular distortions and hydrogen bonding in the intramolecular and intermolecular charge transport of $[NHEt_3]_4[V_8^{IV}V_4^{V}As_8O_{40}(H_2O)]\cdot H_2O$.

DOI: 10.1103/PhysRevB.74.014411 PACS number(s): 75.50.Xx, 78.30.−j, 78.40.−q, 78.67.−n

I. INTRODUCTION

Strong electron correlations, transition metal flexibility, and a rich variety of structural arrangements are at the heart of the novel magnetic, electronic, and catalytic properties of polyoxovanadates. Molecule-based magnets in this family are particularly interesting as the interplay between charge and magnetism, as well as size, shape, and intermolecular distance effects, can be tuned and explored. Among the vanadium-oxygen clusters $[NHEt_3]_4[V_{12}As_8O_{40}(H_2O)]\cdot H_2O$ [abbreviated as $V_{12}(8:4)$] and the chemically similar $[NHEt_3]_3[V_{12}As_8O_{40}(HCO_2)]\cdot 2H_2O$ [henceforth, $V_{12}(6:6)$] have attracted attention as mixed valent systems situated at the crossroads between well-coupled materials such as $K_6[V_{15}As_6O_{42}(H_2O)]\cdot 8H_2O$ (V_{15} for short) and smaller clusters where the magnetic exchange interaction is relatively weak.[1–7]

Figure 1(a) shows the molecular structure of the $[V_8^{IV}V_4^{V}As_8O_{40}(H_2O)]^{4-}$ cluster anion, the building block of $V_{12}(8:4)$. It consists of a V^{4+} central square capped by slightly distorted, mixed-valent squares, with an effective formal 4.5+ oxidation state.[1,5–7] The vanadium squares are bridged by diarsenite ($As_2O_5^{4-}$) groups, and there is a slight asymmetry to the structure due to the displacement of one of the octahedral vanadium centers toward the encapsulated water molecule.[7] The anionic building block of the $V_{12}(6:6)$ material is slightly different [Fig.1(b)]. The molecular skeleton of $V_{12}(6:6)$ closely matches that of $V_{12}(8:4)$, with only slight variations in bond lengths and angles. The V^{4+} central square is, however, capped by mixed-valent squares, each containing one V^{4+} and three V^{5+} centers. Since all vanadium centers are VO_5 in nature and no structural displacement is observed, the anion is more representative of pseudo-D_{4h} symmetry than its 8:4 counterpart. The $V_{12}(6:6)$ structure is also more "well-packed" than the $V_{12}(8:4)$ compound due to the larger size of the encapsulated formate anion.[1,5–7] The magnetic behavior correlates with the geometry and topology of the clusters.[5,6] The spin gap of $V_{12}(8:4)$ is 17.6 K.[8]

The polyoxovandates are different from $[Mn_{12}O_{12}(CH_3COO)_{16}(H_2O)_4]\cdot 2CH_3COOH\cdot 4H_2O$, henceforth Mn_{12}-acetate, and $[Fe_8O_2(OH)_{12}(tacn)_6Br_8]\cdot 9H_2O$, Fe_8Br_8 for short,[9] in that the total spin per molecule as well as the molecular anisotropy are typically small (or even zero). On the other hand, they share common scientific issues such as the development of magnetostructural correlations,[10,11] reconciliation of various experimental and theoretical determinations of the gap, understanding the role of localized and delocalized spin and charge effects, and the microscopic understanding of various conduction pathways.

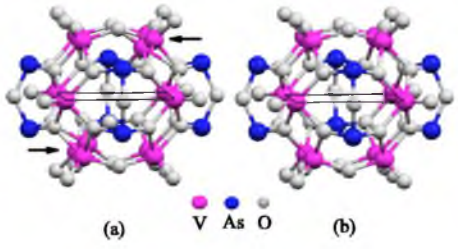

FIG. 1. (Color online) (a) Chemical structure of the $[V_8^{IV}V_4^{V}As_8O_{40}(H_2O)]^{4-}$ cluster anion, the building block of the molecule-based magnet $[NHEt_3]_4[V_8^{IV}V_4^{V}As_8O_{40}(H_2O)]\cdot H_2O$. Note that only one vanadium center is displaced in a cluster, but the sites depicted by arrows occur with equal probability (Ref. 7). (b) Chemical structure of the $[V_6^{IV}V_6^{V}As_8O_{40}(HCO_2)]^{3-}$ cluster anion, the building block of the molecule-based magnet $[NHEt_3]_3[V_6^{IV}V_6^{V}As_8O_{40}(HCO_2)]\cdot 2H_2O$. The dark solid lines identify the inner square of V^{4+} ions in both clusters.

These challenges motivate our cooperative investigation of the transport, optical, and electronic structure properties of the mixed valent $V_{12}(8:4)$ and $V_{12}(6:6)$ materials and allow direct comparison to similar results in V_{15},[12–18] where all of the vanadium centers have 4+ charge, and the cluster has a spin compensated $S=1/2$ ground state.[2–4] Trends between these chemically similar materials are consistent, although the exact value of the gap depends on the nature of the experimental probe and its associated length scale. Specifically, we find that the gap in $V_{12}(8:4)$ is substantially larger than that in $V_{12}(6:6)$ and V_{15}, an effect that can not be explained by molecular distance arguments. The larger value of on-site Coulomb interaction required to account for optical data in $V_{12}(8:4)$ points toward the importance of local charge interactions and electron correlation effects for determining molecular properties in these mixed valent systems, and the observed activated transport reflects both individual cluster characteristics as well as the subtle organization of molecular structure. These issues have been of continuing interest in Mn_{12}-acetate and Fe_8Br_8 as well.[19–21]

II. METHODS

A. Crystal growth

The $V_{12}(8:4)$ and V_{15} samples were synthesized following the optimized procedures described in Refs. 7 and 22. The $V_{12}(6:6)$ crystals were synthesized using a novel method employing slightly higher reaction temperatures, shorter reaction times, and slightly lower reagent concentrates than in previously reported work.[22] These reaction parameters were optimized to yield large and pure crystals of the described compounds. Care was taken to avoid air exposure since the compounds are slowly oxidized by oxygen.

B. Transport measurements

Direct current (dc) conductivity measurements were made on $V_{12}(8:4)$ single crystals using methods described previously for Mn_{12}-acetate, Fe_8Br_8,[23] and V_{15}.[13] Both constant current and constant voltage modes were employed, using a conventional four probe technique. A high input impedance (2×10^{14} ohm) electrometer was needed since the samples showed high resistance ($\approx10^{10}$ ohm) at ambient temperatures. The current-voltage characteristics were periodically checked to verify ohmic behavior in the temperature range 270 to 330 K. At the lower temperature end the resistance became too high to measure with our apparatus. The samples were coated with polymethylmethacrylate after attaching the electrodes in order to obviate the loss of solvent at temperatures above 310 K. The coating technique led to reproducible results over at least two temperature cycles, although the $V_{12}(6:6)$ crystals were too small for this technique.

C. Optical measurements

Near normal polarized and unpolarized reflectance measurements were carried out over a wide frequency range (30–50 000 cm^{-1}; 3.7 meV–6.2 eV) using several different spectrometers including a Bruker 113V Fourier transform infrared spectrometer, a Bruker Equinox 55 Fourier transform infrared system equipped with an infrared microscope, and a Perkin Elmer Lambda-900 grating instrument. The spectral resolution was 2 cm^{-1} in the far and middle infrared and 3 nm in the near-infrared, visible, and near-ultraviolet. The majority of spectra were collected at 300 K, although selected low temperature studies complemented this work. The measurements were carried out on freshly grown single crystals of $V_{12}(8:4)$ and $V_{12}(6:6)$ as well as pressed powder samples of $V_{12}(6:6)$. For the single crystal measurements, we concentrated on the large (110) and (001) faces of $V_{12}(8:4)$ and $V_{12}(6:6)$, respectively. The polarizers/analyzers (wire grid, film, crystal, as appropriate) were positioned to record spectra in the two directions of greatest optical anisotropy on each face, corresponding to the c and $\perp c$ directions for $V_{12}(8:4)$ and the a and $\perp a$ directions for $V_{12}(6:6)$. A Kramers-Kronig analysis was used to calculate the optical conductivity from the measured reflectance, yielding information on the lossy response of the material.[24]

D. Electronic structure calculations

To calculate the electronic and magnetic intramolecular structure of V_{12} we use the atomic sphere approximation (ASA) linear muffin-tin orbitals (LMTO) local spin density approximation plus U (LSDA+U) method. This method accounts for the electronic correlations caused by the on-site Coulomb repulsion between the electrons (the strength of the repulsion is determined by the parameter U). Such correlations are known to be important for numerous metal-oxide crystalline systems, and for the metal-oxide-based magnetic molecules. In particular, the LSDA+U method has been successfully used before[14,15] for studying the molecular magnet V_{15}, and produced good agreement with experimental data. Therefore, we expect that the LSDA+U approach will also be applicable to the similar molecular magnet V_{12}. In our calculations we used a Stuttgart TB-47 code, and the details of the calculations are described in Refs. 14 and 15.

III. RESULTS AND DISCUSSION

A. Transport properties of V_{12}

The inset of Fig. 2(a) shows the resistance of $V_{12}(8:4)$ as a function of temperature under constant voltage conditions (250 V). The resistance increases rapidly with decreasing temperature, exhibiting activated behavior over the 300–270 K range. At 270 K, currents become lower than the threshold of error, restricting our analysis to this temperature range. The 30–40 K temperature window is not wide enough to be able to derive a precise value of the activation energy. However, the activated behavior is clear. An Arrhenius analysis of the accessible regime [(i.e., $R=R_0\exp(-E_a/RT)$], shown in the main panel, yields an activation energy of 0.47 ± 0.05 eV.

As shown in the inset of Fig. 2(b), similar behavior was found at slightly higher temperatures under conditions of constant current.[21,13] Resistance values are on the order of 10^{10} Ω at room temperature and decrease rapidly upon heating. Below 305 K, the resistance of the sample exceeds the

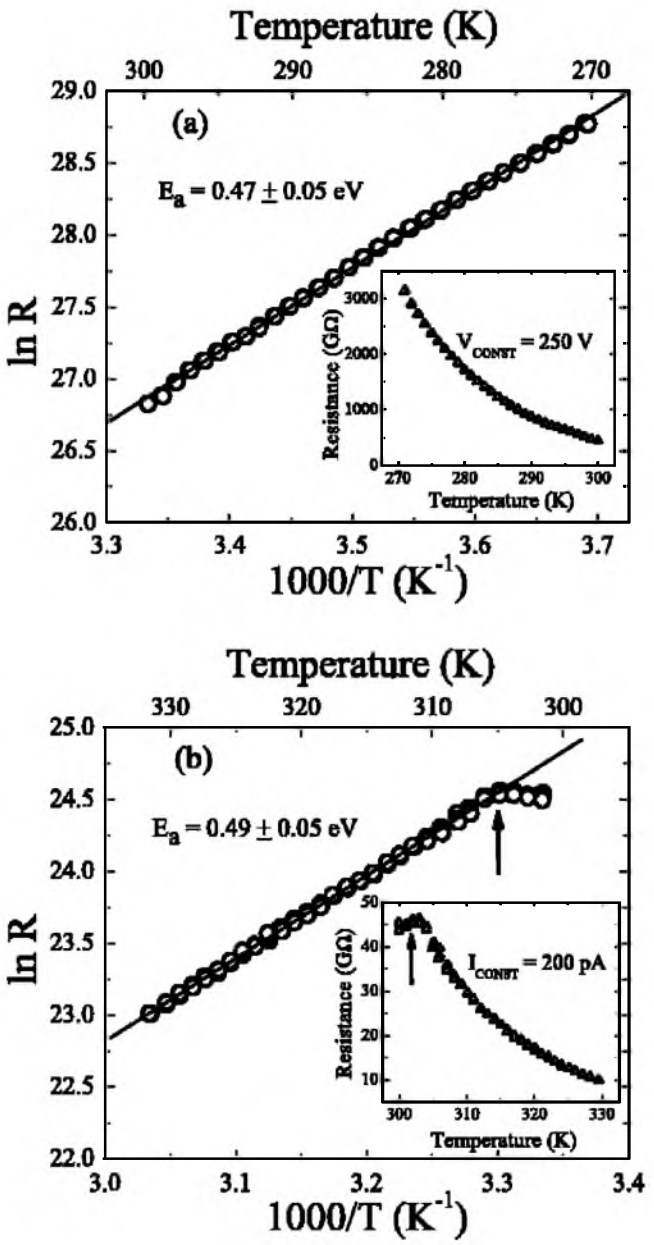

FIG. 2. (a) ln R vs 1/T curve for $V_{12}(8:4)$, which yields an activation energy $E_a=0.47\pm0.05$ eV. The inset shows the temperature dependence of the resistance under constant voltage (250 V). (b) Arrhenius analysis of the resistance of $V_{12}(8:4)$ yields an activation energy of 0.49 ± 0.05 eV. The constant R regime below 305 K (highlighted by arrow) is ascribed to the voltage limit of the current source being exceeded (see text). The inset shows the temperature dependence of the resistance at a constant current (200 pA).

voltage limit of the current source and thus the resistance appears to be constant, as indicated by the arrows in Fig. 2(b). Therefore, under constant current conditions, we are able to characterize the bulk transport $V_{12}(8:4)$ only at temperatures above 305 K. Again, $V_{12}(8:4)$ shows activated behavior from 305 to 330 K, as the resistance rapidly decreases with increasing temperature. Above 305 K, an Arrhenius analysis yields an activation energy of 0.49 eV. The activated transport behavior in $V_{12}(8:4)$ establishes it as a semiconductor with a transport gap $2\Delta=2E_a=0.96\pm0.05$ eV, as shown in Table I.

Figure 3 summarizes the proposed conduction pathway of the two V_{12} materials and the V_{15} analog, derived from the observation of activated transport combined with a careful analysis of the crystal structures. Based upon the large value of the transport gap, we propose that bulk transport in $V_{12}(8:4)$ takes place by direct electron transfer between clusters. The small intercluster distances along the (100) axis (2.918 Å), coupled with few dipolar molecules or ions to facilitate electrical transport, suggests that conduction electrons engage in a direct transfer of electron density between $V_{12}(8:4)$ clusters. This direct mechanism is consistent with the higher resistance seen in $V_{12}(8:4)(\geq10^{10}\ \Omega)$ compared to that of a similar polyoxovanadate compound V_{15} ($10^9\ \Omega$), where although intercluster separations are larger (~3.3 vs 2.918 Å), conduction is facilitated by intercluster ions and molecules.[13] Other transition metal clusters such as $Fe_8Br_8$and Mn_{12}-acetate also display lower resistivity values than $V_{12}(8:4)$ despite larger intercluster separations, due to the presence of ions or dipolar molecules between adjacent clusters,[21] further supporting the direct transfer mechanism in this material.

We were, unfortunately, unable to make resistivity measurements on $V_{12}(6:6)$ because of the lack of sufficiently large single crystals.[25] We can, nevertheless, suggest a possible transport pathway based on details of the crystal packing, optical measurements, and theoretical calculations. $V_{12}(6:6)$ has a similar number of dipolar molecules and ions as $V_{12}(8:4)$, but the crystal structures of the two systems are very different. $V_{12}(8:4)$ is monoclinic[7,26] with $Z=2$, with respect to the clusters; however, six different clusters are involved in the unit cell.[7] In the case of $V_{12}(6:6)$, the unit cell is triclinic[27] with $Z=1$, and there is one cluster centered in the unit cell.[22] The shortest cluster to cluster distance for $V_{12}(6:6)$ is 3.193 Å, with cluster connections beginning with an arsenic and ending at the oxygen of As_2O. However, upon consideration of the smaller unit cell volume and the van der Waals distances in $V_{12}(6:6)$, the most plausible con-

TABLE I. Transport, optical, and theoretically calculated gaps for solid $V_{12}(8:4)$, $V_{12}(6:6)$, and V_{15}.

Material	Magnetic centers	Ground state	$2\Delta_{trans}$ (eV)	$2\Delta_{dielect}$ (eV)	$2\Delta_{opt}$ (eV)	$2\Delta_{opt,peak}$ (eV)	$2\Delta_{theor}$ (eV)
$V_{12}(8:4)$	$V^{4+}:V^{5+}$, $s=1/2$, 0	$S=0$	0.96		1.2±0.1	1.6±0.1	1.5 ($U=6$)
$V_{12}(6:6)$	$V^{4+}:V^{5+}$, $s=1/2$, 0	$S=0$			0.8±0.1	1.3±0.1	1.0($U=4$)
V_{15}	V^{4+}, $s=1/2$	$S=1/2$	0.4 (Ref. 13)	0.44[a]	0.5±0.1 (Ref. 16)	1.2±0.1 (Ref. 16)	1.2 ($U=0$) (Ref. 18) 1.4 ($U=4.2$) (Ref. 14)

[a]The dielectric relaxation gap is obtained from the α-relaxation mode (Ref. 13).

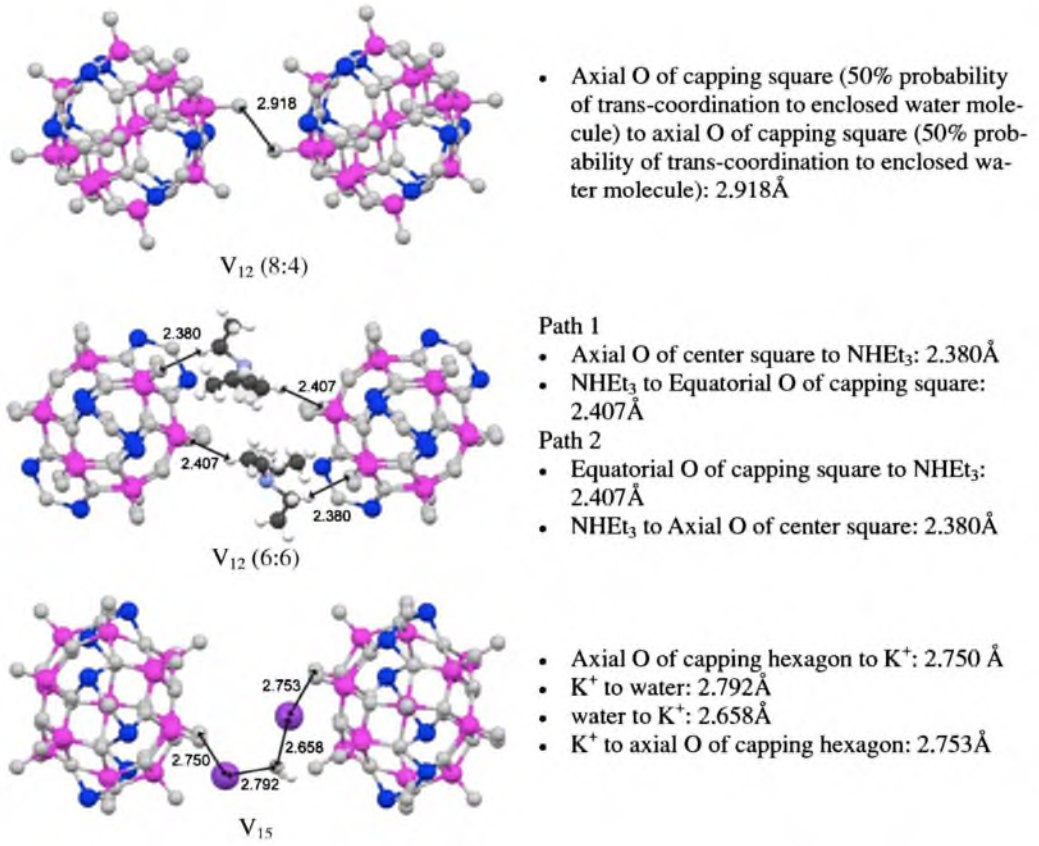

FIG. 3. (Color online) Proposed intermolecular conduction pathways for solid $V_{12}(8:4)$, $V_{12}(6:6)$, and V_{15}. The color/greyscale scheme is the same as in Fig. 1, and the conduction pathway for V_{15} was first proposed in Ref. 13.

duction pathway involves counterions rather than direct intercluster charge transfer. The shortest intermolecular charge transfer pathway has two identical channels. Path 1 originates from an axial oxygen on the central vanadium square of the first cluster, goes to $NHEt_3$ (2.380 Å), and connects with an equatorial oxygen of a capping square (2.407 Å) on the second cluster. Path 2, originating from the first cluster, is identical to path 1, except it is in reverse order, that is, path 2 begins at an equatorial oxygen in the capping square. Charge transfer along these routes roughly occurs through the unit cell vertices, parallel to the cluster's primary axis. These pathways are summarized in Fig. 3; they are considered to be in accord with the following optical and theoretical results.

B. Optical properties

The optical properties of $V_{12}(8:4)$ and $V_{12}(6:6)$ provide a more local view of the charge degrees of freedom. Figure 4 displays the optical conductivity of the V_{12} compounds compared to that of V_{15}.[16] As with many other polyoxovanadates, all materials are Mott insulators. $V_{12}(8:4)$ displays a well-defined optical gap at 1.2 eV and a peak at ~1.6 eV, quite different from the broad leading edge of the excitation (and lower maximum) in V_{15}. The electronic structure of $V_{12}(6:6)$ is comparable with $V_{12}(8:4)$, but the optical gap of $V_{12}(6:6)$ at 0.8 eV and peak at ~1.3 eV is more similar to V_{15}. The excitations between 1 and 2 eV are charge transfer in nature for mixed-valent $V_{12}(8:4)$ and $V_{12}(6:6)$, whereas they display d to d character in V_{15}, especially near the leading edge of the band.[14,15,18] These excitations originate from the V^{4+} capping squares in both V_{12} molecules. While the optical gap should be experimentally determined by extrapolation of the leading edge of the rising conductivity, the peak marks $\Delta k=0$ transitions and the maximum in the joint density of states. The peak value should thus be compared with theoretical predictions (Table I). The features above 3 eV in Fig. 4 are assigned as $Vd \rightarrow Op$ charge transfer excitations. All of these excitations are fairly diffuse, riding on a rising background absorption that reflects the complex and multifaceted density of states of this material. Overall, the measured spectra are in excellent agreement with the calculated electronic structure, as discussed in the next section. These results demonstrate that while the magnetic properties of $V_{12}(8:4)$ and $V_{12}(6:6)$ are dominated by the central antiferromagnetically coupled square,[7,8] the electronic structure is governed by the mixed valent caps. In the polyoxovanadates of interest here, the transport gap is slightly less than the optical gap. This typical result is also observed in Mn_{12} acetate.[19,21] Fe_8Br_8 is an important exception.[20] Here, the transport gap coincides with the extrapolated value of the O p to Fe d charge transfer bands in the optical conductivity.

The vibrational properties of $V_{12}(8:4)$, $V_{12}(6:6)$, and V_{15} are summarized in Table II. The modes affected by hydrogen bonding are particularly interesting. As pointed out by Basler

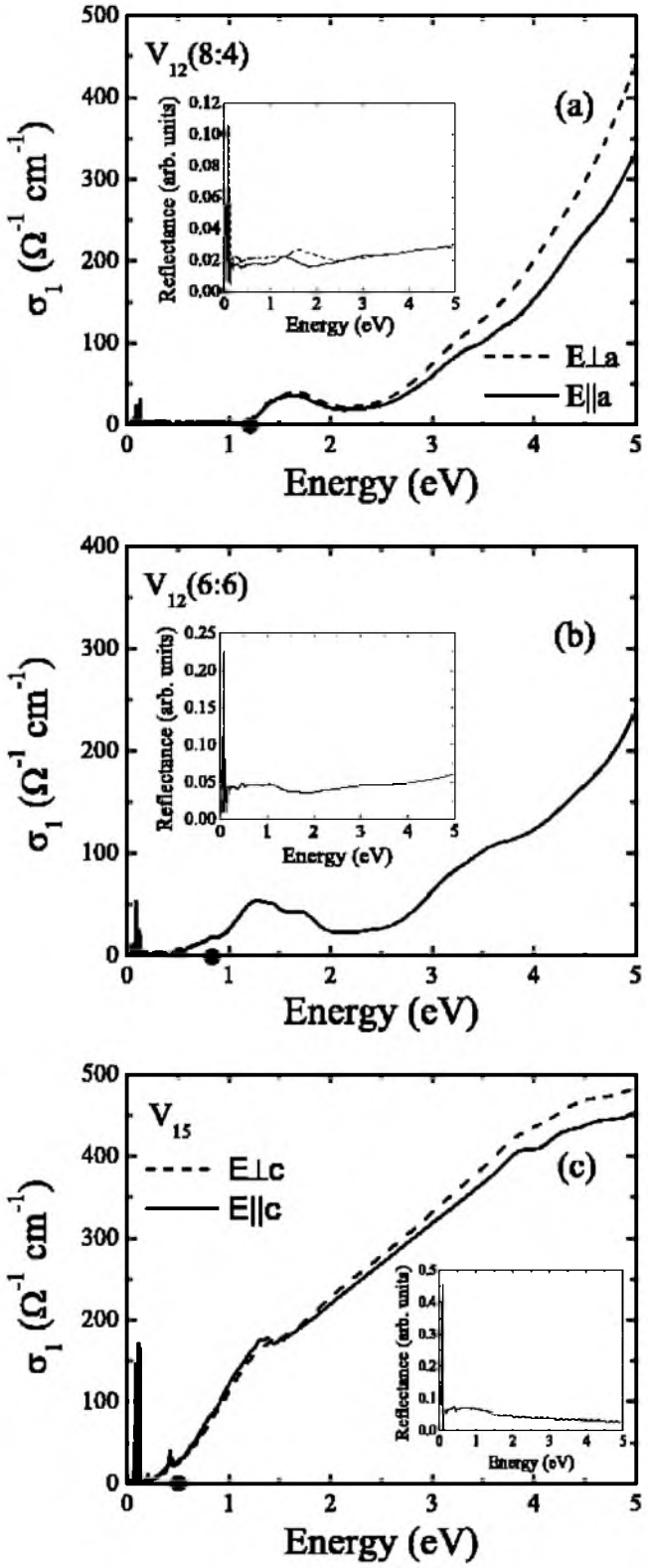

FIG. 4. 300 K optical conductivity, obtained via Kramers-Krönig analysis of the measured reflectance (insets), of (a) $V_{12}(8:4)$, (b) $V_{12}(6:6)$, and (c) V_{15}. Filled circles denote the optical gaps.

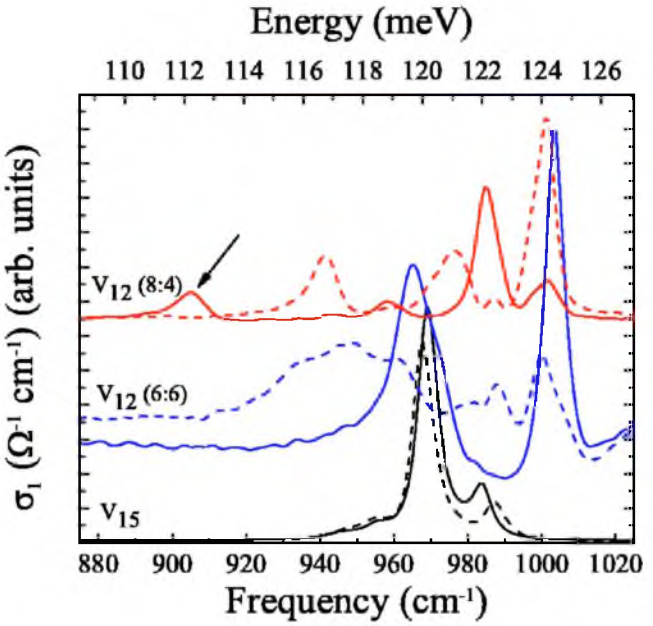

FIG. 5. (Color online) Close-up view of the 300 K optical conductivity of $V_{12}(8:4)$, $V_{12}(6:6)$, and V_{15}, concentrating on the axial V-O stretching modes. Here, solid (dashed) lines indicate that the electric field is applied parallel (perpendicular) to the *a* direction for $V_{12}(8:4)$, parallel (perpendicular) to the *a* direction for $V_{12}(6:6)$, and parallel (perpendicular) to the *c* direction for V_{15}. Spectra are vertically offset and the intensity of the V_{15} data is scaled by a factor of 0.2 for clarity.

et al.,[7] the encapsulated water molecule of $V_{12}(8:4)$ exhibits hydrogen bonding with the molecular cage at the inward V-O bond of the displaced VO_6. Direct evidence of hydrogen bonding is observed in the V-O stretching region. Figure 5 displays a close-up view of the infrared response in this region. Of the numerous features, those above 114 meV are axial V-O stretching modes.[28,29] From bond length evaluation, excitations below 110 meV are equatorial V-O stretching modes. Notably, $V_{12}(8:4)$ has a peak at 112.2 meV (905 cm^{-1}), which is a redshifted axial V-O stretch. The position of this peak can be explained by hydrogen bonding of the encapsulated water molecule.[28,29] Preliminary variable temperature measurements show multiple axial V-O mode splitting, indicating a low temperature distortion of the molecular cage.

Analysis of the rattling motion also provides evidence for hydrogen bonding between the encapsulated H_2O molecule and the cage in $V_{12}(8:4)$. The Einstein model is often used to describe rattlers in open framework materials such as clathrates, filled skudderudites, and β-pyrochlores[30] and can be correlated to atomic displacement parameters as $U_{iso} = h^2T/(4\pi^2 m k_B \Theta_E^2)$. Here, $U_{iso} = \langle U \rangle$, where $\langle U \rangle$ is the mean square displacement amplitude, Θ_E is the Einstein temperature, k_B and h are Boltzmann and Planck constants, m is the reduced mass, and T is the temperature.[30,31] Choi *et al.* also applied this model to predict the rattling frequency of sodium ions encapsulated in vanadium oxide nanotubes.[32] As a consequence, we anticipate that this model for confined low-frequency rattling will work well for these chemically similar polyoxovanadate clusters. The predicted rattling frequencies for H_2O encapsulated by $V_{12}(8:4)$ and V_{15} are 9.6 meV, for each. For $V_{12}(6:6)$, the predicted rattling fre-

TABLE II. Vibrational mode assignments for $V_{12}(8:4)$, $V_{12}(6:6)$, and V_{15}. Many ligand-related features appear at higher energies.

$V_{12}(8:4)$ peak position in meV (cm^{-1})	Polarization	$V_{12}(6:6)$ peak position in meV (cm^{-1})	Polarization	V_{15} peak position in meV (cm^{-1})	Polarization	Assignment
124.2 (1002)	$E\|a$, $E\perp a$	124.4 (1003)	$E\|a$	122.4 (987)	$E\perp c$	V-O (axial)
122.4 (987)	$E\perp a$	124.0 (1000)	$E\perp a$	122.0 (984)	$E\|c$	stretching
122.1 (985)	$E\|a$	122.5 (988)	$E\perp a$	120.0 (968)	$E\|c$, $E\perp c$	
121.1 (977)	$E\perp a$	119.7 (965)	$E\|a$	118.4 (955)	$E\|c$, $E\perp c$	
118.9 (959)	$E\|a$	119.2 (961)	$E\perp a$	117.4 (947)	$E\|c$	
116.7 (941)	$E\perp a$	117.7 (949)	$E\perp a$			
112.2 (905)[a]	$E\|a$					
104.2 (840)	$E\|a$	99.9 (806)	$E\|a$	98.5 (794)	$E\perp c$	V-O (equatorial)
101.2 (816)	$E\perp a$	99.7 (804)	$E\perp a$	92.3 (744)	$E\|c$, $E\perp c$	stretching
89.9 (725)	$E\|a$	86.3 (696)	$E\perp a$	89.2 (719)	$E\|c$	
88.5 (714)	$E\perp a$	85.8 (692)	$E\|a$	88.8 (716)	$E\perp c$	
86.2 (695)	$E\|a$			85.6 (690)	$E\|c$, $E\perp c$	
				82.8 (668)	$E\|c$, $E\perp c$	
75.1 (606)	$E\|a$	75.1 (606)		78.7 (635)	$E\|c$	As-O stretching
		65.0 (524)		78.2 (631)	$E\perp c$	
58.0 (468)	$E\|a$, $E\perp a$	56.7 (457)		59.3 (478)	$E\|c$	V-O bending
46.3 (373)	$E\|a$, $E\perp a$	46.5 (375)		58.5 (472)	$E\perp c$	
		43.3 (349)		48.4 (390)	$E\|c$, $E\perp c$	
35.1 (283)	$E\perp a$	35.5 (286)		36.6 (295)	$E\|c$, $E\perp c$	As-O bending
34.7 (280)	$E\|a$	31.1 (251)				
30.3 (244)	$E\|a$, $E\perp a$					
18.4 (148)	$E\|a$	15.8 (128)		21.9 (177)	$E\|c$, $E\perp c$	
18.0 (145)	$E\perp a$					
15.7 (127)	$E\|a$					
13.5 (109)	$E\perp a$	12.6 (102)		10.5 (85)	$E\|c$, $E\perp c$	rattling
13.1 (106)	$E\|a$					motion

[a]Redshifted due to hydrogen bonding with the encapsulated water molecule (Refs. 7 and 28).

quency of formate is 12.2 meV. This compares with observed values of 13.5 meV (H_2O), 12.6 meV (HCO_2^-), and 10.5 meV (H_2O) for $V_{12}(8:4)$, $V_{12}(6:6)$, and V_{15}, respectively. The large difference between predicted and observed values in $V_{12}(8:4)$ suggests that motion of the water molecule in this material is more restricted. The other values are in good agreement with predictions from this simple rattling model. Clearly, the local distortion and associated hydrogen bonding in $V_{12}(8:4)$ have subtle but important effects on the intramolecular charge transfer. Rattler/cage mixing effects are of future interest.

C. Theoretical results

LSDA calculations have been performed for both $V_{12}(6:6)$ and $V_{12}(8:4)$, for different values of U. In Figs. 6 and 7, we present the calculated partial densities of states (DOS) of vanadium $3d$ and oxygen $2p$ electrons for $U=0$, 4, 5, and 6 eV, for the compounds $V_{12}(6:6)$ and $V_{12}(8:4)$. For $U=0$, both compounds exhibit nonzero electron density at the Fermi level, thus demonstrating the importance of the on-site Coulomb repulsion (finite value of U) for adequately describing V_{12}. For sufficiently large U (4–6 eV), both compounds exhibit a pronounced gap, and two well-isolated peaks in the V $3d$ DOS are clearly seen. The origin of these peaks can be understood from Figs. 8 and 9, where the partial V $3d$ DOS corresponding to different positions of the vanadium atoms are presented. The two isolated peaks come from the electrons localized on V^{4+} sites situated in the central square (the lower peak) and in the capping squares (the higher peak). Along with the peaks, the vanadium $3d$ DOS exhibits broad bands located approximately between −2 and −8 eV. These features correspond to the electrons delocalized over the molecule, and demonstrate the significant hybridization between the V d and the O p states. The peaks corresponding to the localized electrons also show some signature of the p-d hybridization, but to a much smaller extent.

With increasing the value of the on-site repulsion parameter U, the gap between the occupied and unoccupied states increases, while the shapes of the DOS do not show qualitative changes. By comparing the values of the gap for different U with the experimental results above, we find that the optimal value of U for $V_{12}(8:4)$ is 6 eV, while for $V_{12}(6:6)$ the optimal value is 4 eV. Such a noticeable difference is somewhat unexpected, so we performed *ab initio* theoretical calculations of the parameter U using the constrained LSDA

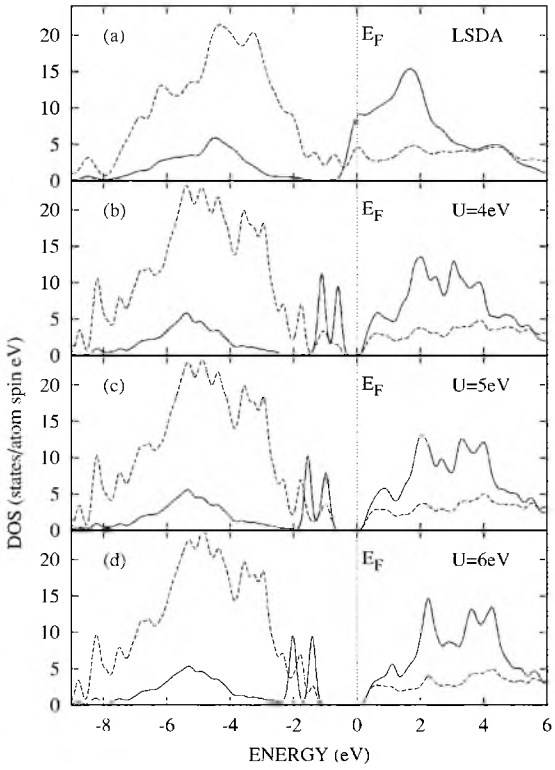

FIG. 6. Dependence of the $3d$ vanadium (solid lines) and $2p$ oxygen (dashed lines) DOS in $V_{12}(8:4)$ on the Coulomb repulsion parameter U, for the values of U from 4 to 6 eV, and $J=0.8$ eV.

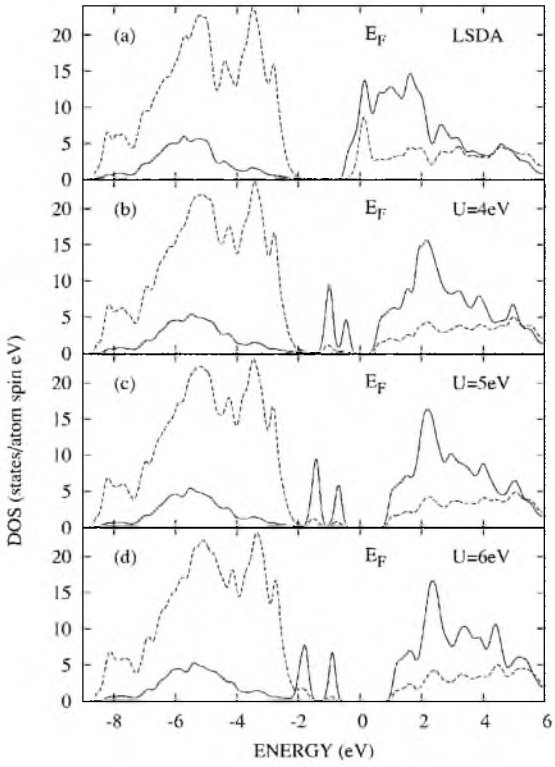

FIG. 7. Dependence of the $3d$ vanadium (solid lines) and $2p$ oxygen (dashed lines) DOS in $V_{12}(6:6)$ on the Coulomb repulsion parameter U, for the values of U from 4 eV to 6 eV and $J=0.8$ eV.

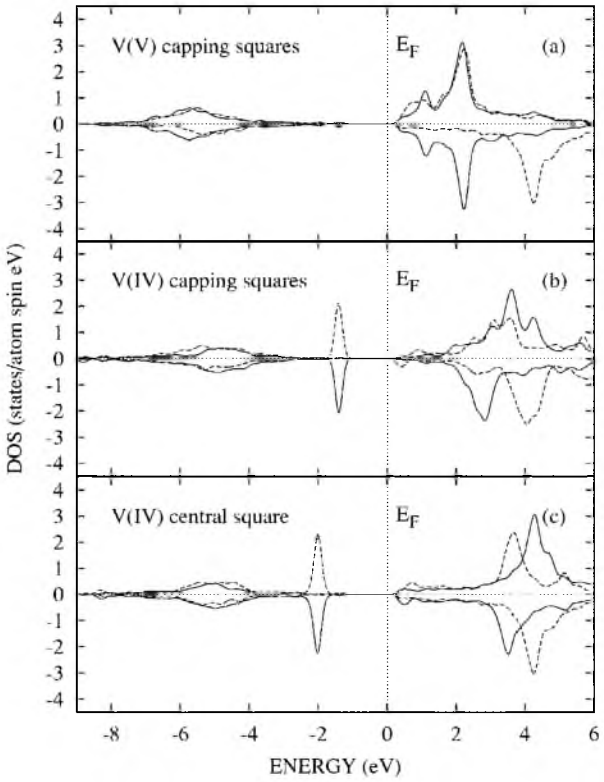

FIG. 8. DOS of d-electrons of inequivalent V ions in $V_{12}(8:4)$. Different types of lines correspond to different structural classes of V ions. The DOS are calculated for $U=6$ eV and $J=0.8$ eV.

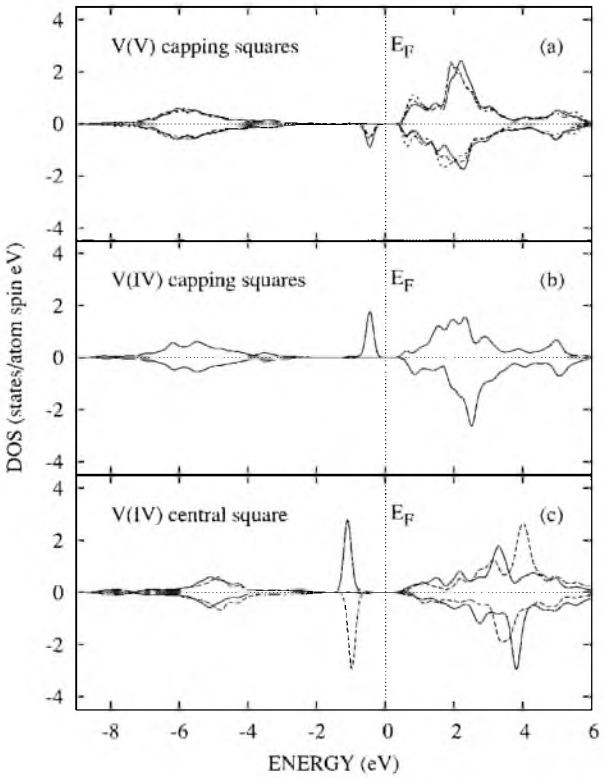

FIG. 9. DOS of d-electrons of inequivalent V ions in $V_{12}(6:6)$. Different types of lines correspond to different structural classes of V ions. The DOS are calculated for $U=4$ eV and $J=0.8$ eV.

TABLE III. Magnetic moments for $V_{12}(8:4)$, $V_{12}(6:6)$, and V_{15} for several values of U.

Cluster	Atom	Charge	Layer	4 eV	5 eV	6 eV
	V_1	+5	capping	−0.05	−0.04	−0.04
	V_2	+5	capping	0.16	0.16	0.15
V_{12}	V_3	+4	capping	−0.91	−0.92	−0.92
(8:4)	V_4	+4	capping	0.87	0.89	0.89
	V_5	+4	central	−1.01	−1.01	−1.01
	V_6	+4	central	1.02	1.02	1.02
	V_1	+5	capping	−0.22	−0.22	−0.21
	V_2	+5	capping	−0.16	−0.16	−0.17
V_{12}	V_3	+5	capping	−0.21	−0.21	−0.20
(6:6)	V_4	+4	capping	0.59	0.59	0.62
	V_5	+4	central	−0.93	−0.94	−0.94
	V_6	+4	central	0.94	0.95	0.95
	V_1	+4	capping	0.94	0.94	0.95
V_{15}[14]	V_2	+4	capping	−0.91	−0.92	−0.93
	V_3	+4	central	1.01	1.02	1.02

calculations as described in Ref. 33. The constrained LDA calculations give a reasonable estimate for the parameter U, but due to the large size of the considered molecules, the resulting value of U is not as accurate as for smaller systems: for a fixed calculation time, the self-consistency conditions for large systems are satisfied with much less precision than for small systems. These calculations gave $U=4.1$ eV for $V_{12}(6:6)$ and $U=5.1$ eV for $V_{12}(8:4)$, i.e., the calculated values of U for both compounds agree reasonably well with the values of U inferred from the comparison with the experiment.

It is interesting to note the similarity between the electronic structure of V_{12} and previously calculated[14,15] electronic structure of a similar polyoxovanadate compound V_{15}. Both DOS and the magnetic moments of vanadium atoms (see Table III) are similar in these materials. Furthermore, the optimal value of U for V_{15} is around 4 eV, as inferred from different experiments (x-ray photoelectron and x-ray fluorescence spectra,[15] optical measurements,[16] and magnetic susceptibility studies[14]), and the independent theoretical estimate (from the constrained LSDA calculations) for V_{15} gives the close value $U=3.8$ eV. These values are close to $U=4$ eV obtained for $V_{12}(6:6)$.

In order to understand the difference in U values between $V_{12}(6:6)$ and $V_{12}(8:4)$, it is useful to compare these compounds with V_{15}. The mutual positions of V $3d$ and O $2p$ DOS in $V_{12}(6:6)$ and in V_{15} are similar, while for $V_{12}(8:4)$ the oxygen p bands are located slightly deeper. As a result, the p-d hybridization in $V_{12}(8:4)$ is weaker than in $V_{12}(6:6)$ and V_{15}. However, the stronger p-d hybridization leads to less localized wave functions, i.e., to the reduced electron density on a given vanadium site, so that the on-site Coulomb repulsion is reduced, resulting in a smaller value of U. Therefore, $V_{12}(8:4)$ molecules exhibiting weaker hybridization have a larger value of U than $V_{12}(6:6)$ and V_{15}, and, correspondingly, the gap in $V_{12}(8:4)$ is larger than in $V_{12}(6:6)$ and V_{15}.

IV. CONCLUSION

We report a joint experimental and theoretical investigation of the transport gap, optical properties, and electronic structure of two chemically similar, mixed-valent polyoxovanadate molecular magnets and compare our results with those of other vanadium cluster-based materials. Trends between these chemically similar materials are consistent, although the exact value of the gap depends on the nature of the experimental probe and its associated length scale. We attribute the substantial gap in $V_{12}(8:4)$ to weak p-d hybridization and a large on-site Coulomb repulsion ($U=6$ eV). The reduced gap in $V_{12}(6:6)$ is associated with a smaller value of U, at least from a molecular point of view, although the transport properties also reflect subtle organization of the molecular structure. Based upon the large value of the gap in $V_{12}(8:4)$, we propose that bulk transport takes place by direct electron transfer between clusters along the (100) axis (2.918 Å). Direct electron transfer is indicated because there are few dipolar molecules or ions to facilitate the charge transfer between clusters in this system. This mechanism is consistent with the higher resistance seen in $V_{12}(8:4)(\geq 10^{10}\ \Omega)$ compared to that of V_{15} ($10^9\ \Omega$), where although intercluster separations are larger (~3.3 Å vs 2.918 Å), conduction is facilitated by intercluster ions and molecules.[13] In $V_{12}(6:6)$, intermolecular charge transfer occurs via counter ions and is also activated. Efforts are underway to grow large enough single crystals of $V_{12}(6:6)$ for charge transport measurements and to assess the mechanism proposed in Table II. A detailed analysis of the vibrational response supports the important role of hydrogen bonding and local molecular distortion in influencing intramolecular charge transport in $V_{12}(8:4)$ as well.

ACKNOWLEDGMENTS

Work at UT was supported by the Petroleum Research Fund administered by the American Chemical Society (Grant No. PRF-AC 38164) and the U.S. Department of Energy (through Ames Lab Subcontract No. A2-3590). Research at FSU is supported by the National Science Foundation (Grants No. NIRT-DMR 0103290 and No. 0506946). Work at the IMP-RAS was partially supported by the Research Council of the President of the Russian Federation (Grant No. NSH-4640.2006.2) and the Russian Foundation for Basic Research (Grant No. RFFI-05-02-17704). Research at Ames Lab was supported by the Director of the Office of Science, Office of Basic Energy Research of the U. S. Department of Energy. Ames Laboratory is operated for the U. S. Department of Energy by Iowa State University under Contract No. W-7405-82.

[1] A. Müller, J. Döring, and H. Bögge, Chem. Commun. (Cambridge) **1991**, 273.
[2] G. Chaboussant, R. Basler, A. Sieber, S. T. Ochsenbein, A. Desmedt, R. E. Lechner, M. T. F. Telling, P. Kögerler, A. Müller, and H.-U. Güdel, Europhys. Lett. **59**, 291 (2002).
[3] A. L. Barra, D. Gatteschi, L. Pardi, A. Müller, and J. Döring, J. Am. Chem. Soc. **114**, 8509 (1992).
[4] I. Chiorescu, W. Wernsdorfer, A. Müller, H. Bögge, and B. Barbara, J. Magn. Magn. Mater. **221**, 103 (2000).
[5] D. Gatteschi, B. Tsukerblat, A.-L. Barra, L. C. Brunel, A. Müller, and J. Döring, Inorg. Chem. **32**, 2114 (1993).
[6] D. Gatteschi and B. S. Tsukerblat, Mol. Phys. **79**, 121 (1993).
[7] R. Basler, G. Chaboussant, A. Siever, H. Andres, M. Murrie, P. Kögerler, H. Bogge, D. C. Crans, E. Krickemeyer, S. Janssem H. Mutka, A. Müller, and H.-U. Güdel, Inorg. Chem. **41**, 5675 (2002).
[8] D. Procissi, A. Shastri, I. Rousochatzakis, M. A. Rifai, P. Kögerler, M. Luban, B. J. Suh, and F. Borsa, Phys. Rev. B **69**, 094436 (2004).
[9] L. Thomas, F. Lionti, R. Ballou, D. Gatteschi, R. Sessoli, and B. Barbara, Nature (London) **383**, 145 (1996); J. R. Friedman, M. P. Sarachik, J. Tejada, and R. Ziolo, Phys. Rev. Lett. **76**, 3830 (1996); J. A. A. J. Perenboom, J. S. Brooks, S. Hill, T. Hathaway, and N. S. Dalal, Phys. Rev. B **58**, 330 (1998); K. Wieghardt, K. Pohl, L. Gibril, and G. Huttner, Angew. Chem., Int. Ed. Engl. **23**, 77 (1984); R. Caciuffo, G. Amoretti, A. Murani, R. Sessoli, A. Caneschi, and D. Gatteschi, Phys. Rev. Lett. **81**, 4744 (1998).
[10] W. Plass, Inorg. Chem. **36**, 2200 (1997).
[11] K. Hegetschweiler, B. Morgenstern, J. Zubieta, P. J. Hagrman, N. Lima, R. Sessoli, and F. Totti, Angew. Chem., Int. Ed. **43**, 3436 (2004).
[12] A. F. Popkov, N. E. Kulagin, A. I. Mukhanova, A. I. Popov, and A. K. Zvezdin, Phys. Rev. B **72**, 104410 (2005).
[13] D. Zipse, N. S. Dalal, R. Vasic, J. S. Brooks, and P. Kögerler, Phys. Rev. B **71**, 064417 (2005).
[14] D. W. Boukhvalov, V. V. Dobrovitski, M. I. Katsnelson, A. I. Lichtenstein, B. N. Harmon, and P. Kögerler, Phys. Rev. B **70**, 054417 (2004).
[15] D. W. Boukhvalov, E. Z. Kurmaev, A. Moewes, D. A. Zatsepin, V. M. Cherkashenko, S. N. Nemnonov, L. D. Finkelstein, Yu. M. Yarmoshenko, M. Neumann, V. V. Dobrovitski, M. I. Katsnelson, A. I. Lichtenstein, B. N. Harmon, and P. Kögerler, Phys. Rev. B **67**, 134408 (2003).
[16] J. Choi, L. A. W. Sanderson, J. L. Musfeldt, A. Ellern, and P. Kögerler, Phys. Rev. B **68**, 064412 (2003).
[17] J. Kortus, C. S. Hellberg, and M. R. Pederson, Phys. Rev. Lett. **86**, 3400 (2001).
[18] J. Kortus, M. R. Pederson, C. S. Hellberg, and S. N. Khanna, Eur. Phys. J. D **16**, 177 (2001).
[19] S. M. Oppenheimer, A. B. Sushkov, J. L. Musfeldt, R. M. Achey, and N. S. Dalal, Phys. Rev. B **65**, 054419 (2002).
[20] T. Baruah, J. Kortus, M. R. Pederson, R. Wesolowski, J. T. Haraldsen, J. L. Musfeldt, J. M. North, D. Zipse, and N. S. Dalal, Phys. Rev. B **70**, 214410 (2004).
[21] J. M. North, D. Zipse, N. S. Dalal, E. S. Choi, E. Jobiliong, J. S. Brooks, and D. L. Eaton, Phys. Rev. B **67**, 174407 (2003).
[22] J. Fielden, A. Ellern, and P. Kögerler (unpublished).
[23] J. M. North, D. Zipse, N. S. Dalal, E. S. Choi, E. Jobiliong, J. S. Brooks, and D. L. Eaton, Phys. Rev. B **67**, 174407 (2003).
[24] F. Wooten, *Optical Properties of Solids* (Academic Press, New York, 1972).
[25] The $V_{12}(6:6)$ crystals were too small for transport measurements using the coating technique.
[26] $V_{12}(8:4)$ unit cell parameters $a=12.239(2)$ Å, $b=21.377(4)$ Å, $c=13.713(2)$ Å, $\alpha=90$, $\beta=111.739(3)$, $\gamma=90$.
[27] $V_{12}(6:6)$ unit cell parameters $a=11.627(2)$ Å, $b=12.595(3)$ Å, $c=13.778(3)$ Å, $\alpha=116.407(3)$, $\beta=96.213(3)$, $\gamma=105.584(4)$.
[28] A. Demšar and O. Bukovec, Inorg. Chim. Acta **25**, L121 (1977).
[29] J. Selbin, L. H. Homes, Jr., and S. P. McGlynn, J. Inorg. Nucl. Chem. **25**, 1359 (1963).
[30] B. C. Sales, D. Mandrus, and B. C. Chakoumakos, *Recent Trends in Thermoelectric Materials Research II*, edited by T. M. Tritt (Academic, New York, 2001), Vol. 70, Chap. 1, pp. 1–34.
[31] Here, these principles were applied to encapsulated water and formate molecules. For H_2O, the atomic displacement parameters for hydrogen were approximated using the spherical area of the Bohr radius, and the formate ion was simplified by using only the area of CO_2. Simple averages provide instructive (but not perfect) results for non-chain-like molecules.
[32] J. Choi, J. L. Musfeldt, Y. J. Wang, H.-J. Koo, M.-H. Whangbo, J. Galy, and P. Millet, Chem. Mater. **14**, 924 (2002).
[33] V. I. Anisimov and O. Gunnarsson, Phys. Rev. B **43**, 7570 (1991).